P9.4 OBSERVATIONS OF SPATIAL VARIATIONS IN CONVECTIVE BOUNDARY LAYER STRUCTURE OVER A HETEROGENEOUS LAND SURFACE DURING IHOP

Songlak Kang* and Kenneth J. Davis
The Pennsylvania State University, Department of Meteorology, University Park, Pennsylvania

1. INTRODUCTION

Interaction between the land surface and the atmosphere has become a widely studied topic in the field of meteorology. An essential part of this interaction is the response of the atmospheric boundary layer (ABL) response to land-surface heterogeneity. For example, Taylor et al. (1997) linked ABL variability induced by antecedent rainfall variability to a favored region for the intensification of a single convective cell. Persistent spatial variability in the ABL, possibly created by land surface heterogeneity, may create favored locations for moist convective initiation.

Due to the difficulty in observing the temporal evolution of two and three dimensional ABL structures, many studies of surface-atmosphere interactions have relied primarily upon numerical simulation (e.g. Weaver and Avissar, 2001; Segal and Aritt, 1992; Avissar and Schmidt, 1998; Shen and Leclerc, 1995). Although some observational studies of the surface-atmosphere interaction exist (e.g. Mahrt et al.,1994 a, b; LeMone et al., 2002), more observations of these interactions are needed. In addition, improvements in technology have expanded our ability to observe complex land-atmosphere interactions.

The International H2O Project (IHOP_2002) was conducted over the Southern Great Plains (SGP) (Weckwerth et al., 2004) with the aim of improving our understanding of convective precipitation, including the development of land-ABL structures that might contribute to this understanding. As a part of experiment, the University of Wyoming King Air (UWKA) flew repeatedly over three tracks with the goal of investigating the effects of a heterogeneous land surface on ABL structure. Among the three UWKA tracks, the western track, a 50-km north-south track, approximately from 36.4 to 37.0 N along 100.6 W, shows the most significant surface heterogeneity. In addition, the daily variability of surface and weather conditions is substantial. Several additional observing systems (flux towers, airborne and ground-based radars, lidars and radiometers) were deployed in addition to the UWKA. The data set collected over the western track provides a great opportunity to study the interaction between land surface and daytime ABL under variable surface and weather conditions.

In this study we document variability in ABL structure caused by land-surface heterogeneity. Using the variance decomposition method of Mahrt et al. (1994b), the stationary spatial patterns are isolated and the importance of surface forcing in creating the ABL structure is assessed.

*Corresponding author address: Songlak Kang, The Pennsylvania State University, Dept. of Meteorology, University Park, PA 16802; email:szk111@psu.edu

2. DATA

The UWKA measurements obtained over the western track during IHOP_2002 are the primary data for this study. Five boundary layer heterogeneity (BLH) missions were flown over this location on 19, 20, 25, 29 May, and 7 June, 2002. During these missions, the UWKA flew 61 legs to measure potential temperature, water vapor mixing ratio, wind direction and magnitude, and other variables. Among these, 30 legs were low-level legs, where the aircraft altitude was approximately 65 m AGL. The other 31 legs were upper-level legs, where the aircraft altitude was higher than 100 m AGL.

The UWKA track flew over three Integrated Surface Flux Facility (ISFF) stations deployed along the western track. These surface flux stations directly measured momentum, sensible and latent heat fluxes as well as standard surface and meteorological variables. These data are used to verify UWKA observations and to understand the causes of land surface heterogeneity.

The DLR (Deutsche Luft und Raumfahrt) Falcon also flew a downward-pointing H_2O differential absorption lidar(Ehret et al., 1998) over the western track during the five BLH missions. From the aerosol backscatter data obtained from this lidar, ABL depth can be estimated using the Haar wavelet technique (Davis et al., 2000).

3. DECOMPOSITION OF THE UWKA DATA

3.1. Stationary Spatial Variability

The UWKA flew repeated low-level legs over the western track during each mission. Time- and space-composited ABL structure is constructed from these low-level legs for each day. Individual low-level legs are divided into spatial segments prior to temporal averaging. The average for the k th segment in the j th leg is calculated over a nonoverlapping window of either 1, 2, 5, 10, or 25 km from UWKA 25 Hz data,

$$\left[\phi\right]_{j,k} = \frac{1}{L}\sum_{i=1}^{L}\phi_i \ , \qquad (1)$$

where $\left[\ \right]$ indicates a segment average and ϕ_i is the i^{th} data point for a particular observed variable (e.g.

temperature, humidity) in segment k of the low-level leg j. L is the number of data points in segment k.

Consequently, stationary spatial variability over the western track during a given day can be described by time-averaging the segment averages over all the low-level legs at location k:

$$\{[\phi]\}_k = \frac{1}{M}\sum_{j=1}^{M}[\phi]_{j,k}, \quad (2)$$

where $\{\ \}$ indicates a time average, j indicates the individual leg and M is the number of low-level legs flown by the UWKA on a given day.

3.2. Variance Decomposition

Following the variance decomposition method of Mahrt et al. (1994b), the significance of persistent spatial variability can be compared with temporal and transient variability. An underlying goal is to study the correlation between persistent spatial variability and land surface heterogeneity. First, the leg average must be obtained from the segment averages (1),

$$\langle\phi\rangle_j = \frac{1}{N}\sum_{k=1}^{N}[\phi]_{j,k}, \quad (3)$$

where $\langle\ \rangle$ indicates a leg average, j indicates an individual leg, N is the number of segments, and k is a segment in leg j.

From the leg average (3), the spatial deviation of the k th segment in the j th leg is defined as

$$\phi^*_{j,k} = [\phi]_{j,k} - \langle\phi\rangle_j \quad . \quad (4)$$

By averaging the spatial deviation over all the low-level legs, the stationary part of the spatial deviation (4) can be obtained from

$$\{\phi^*\}_k = \sum_{j=1}^{M}\phi^*_{j,k} \ . \quad (5)$$

Further, the transient part of the spatial deviation is defined by the difference between the stationary part of the spatial deviation (5) and the spatial deviation (4) at the k th segment in the j th leg, or

$$\phi^{*'}_{j,k} = \phi^*_{j,k} - \{\phi^*\}_k \ . \quad (6)$$

From (3), (5), and (6), Mahrt et al. (1994) presented the following variance decomposition,

$$\left\{\left\langle[\phi]^2\right\rangle\right\} = \left\{\langle\phi\rangle^2\right\} + \left\langle\left\{\phi^*\right\}^2\right\rangle + \left\{\left\langle\phi^{*'2}\right\rangle\right\}. \quad (7)$$

Prior to these operations the global average, $\{\langle[\phi]\rangle\}$, was removed from the segment average (1). Therefore (7) represents a decomposition of the total variance of the segments. The total variance (left hand side of (7)) of the local segments of the low-level legs on a given day can be divided into three parts (in order, on the right hand side of (7)): temporal variability of the leg average, the stationary part of the spatial deviation from the leg average, and the transient part of the spatial deviation from the leg average.

4. SURFACE AND ABL VARIABILITY

4.1. Surface Variability

Applying (2) to the low-level legs of the UWKA, we created composite maps of surface heat and moisture flux, and radiation temperature along the flight track. Along with these composites, the significance of stationary spatial variability is assessed using the variance decomposition (7). Five different segment lengths (1, 2, 5, 10, and 25 km) are examined to identify characteristic length scales of surface-ABL interactions. The number of UWKA low-level flight passes on a given day ranged from 2 to 10. On 25 May, a high pressure system passed across the western track and caused a significant wind shift. The low-level flight passes on 25 May are therefore divided into the two parts, 25A and 25B, where each part has five low-level flight legs.

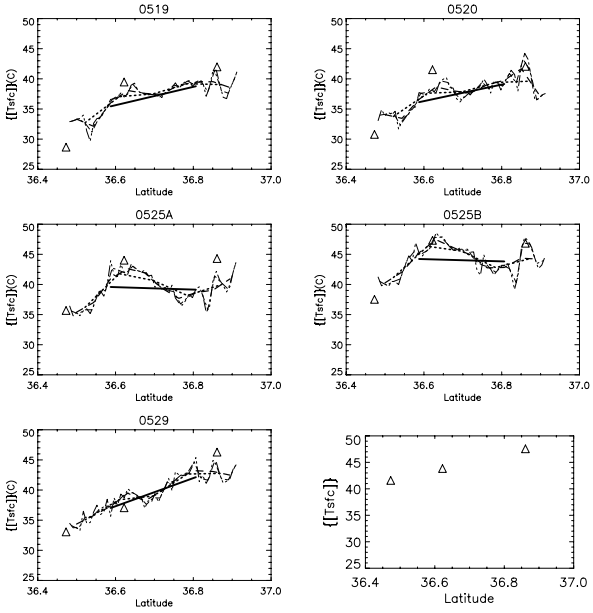

Fig.1. Composite structures of surface IR radiometric temperature using 1-(dot-dot-dashed), 2-(dot-dashed), 5-(dashed), 10-(dotted), and 25-(solid) km segment averages from the low-level legs of the UWKA over the western IHOP flight track. The numbered triangles indicate the surface temperature measured at the ISFF station 1, 2, and 3 from south to north. On 7 June there is no aircraft measurement of IR radiometric temperature due to a breakdown of the radiometer.

In Fig.1 warmer surface IR temperatures to the north and cooler conditions to the south were persistent through all the cases. This feature can be described

simply by the 25-km segment averages. However, on 25 May, the spatial variability described by the 25-km averages seems to be inappropriate. The spatial pattern of the relatively warm region around 36.65 N and the relatively cool region around 36.75 N described by the 10-km or shorter segment averages captures the primary characteristics of the surface radiation temperature distribution.

Surface heterogeneity influences the ABL via heterogeneity of surface heat and moisture fluxes. The fluxes computed from airborne eddy-covariance measurements vary depending on the segment length (or cutoff length) as well as the computational method. Sun et al. (1996) suggested that the flux based on a cutoff length of 1 km best represents the turbulent flux that can be well described by bulk aerodynamic methods. They reported that segment lengths longer than 1 km can include non-turbulent motions. In this study, the segment lengths of 1, 2, 5, 10 and 25 km are used for defining the perturbations. Therefore the surface heat and moisture flux distribution may include fluxes caused by non-turbulent motions on the horizontal length scale larger than the segment length but smaller than the flight leg length (about 50 km).

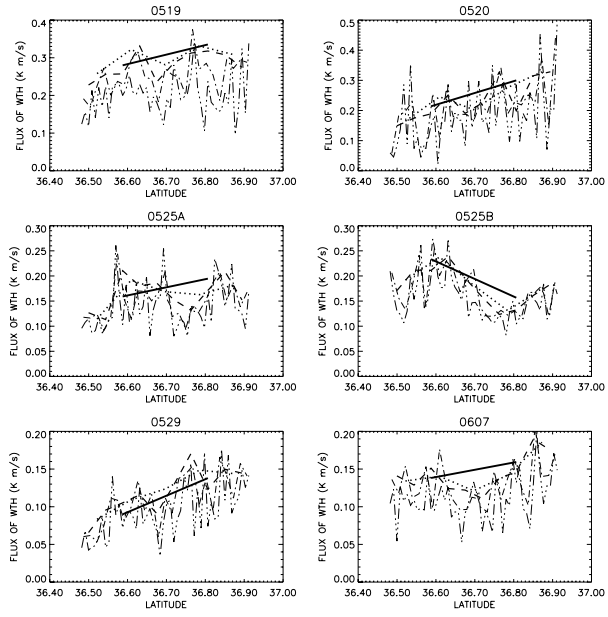

Fig. 2. Same as Fig.1 but for surface kinematic heat flux

A consistent pattern of larger kinematic heat flux to the north and smaller flux to the south is apparent in the surface heat flux distribution (Fig. 2). This pattern persists regardless of the cutoff length scale, except on 25A May, where the surface heat flux distribution shows significant differences depending on the cutoff length scale, especially with the 25 km length scale. The spatial pattern of the surface sensible heat flux described by 5 or 10 km segment averages on 25A May and by 10 or 25 km segment averages on 25B May are the largest segments possible that still capture most of the stationary spatial patterns. Variance decomposition shows much larger normalized spatial variance values on 25 May than for other cases. Thus, the spatial pattern on 25 May seems to be more stationary and more significant than on the other days.

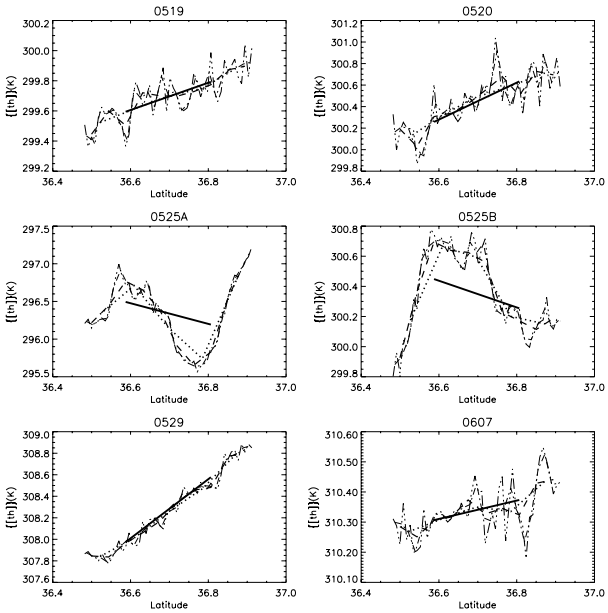

Fig. 3. Same as Fig.1 but for potential temperature at 65 m AGL

Moisture fluxes show a pattern of high fluxes to the south and drier conditions to the north persistent for all the cases that is consistent with the surface temperature and sensible heat flux results. Variance decomposition, however, suggests that the spatial pattern of surface moisture flux is much less stationary than that of surface heat flux, except on 19 May. In other words, the spatial pattern of the moisture flux is more transient than the spatial pattern of sensible heat flux.

4.2 ABL Variability

Depending on ambient conditions such as friction velocity, mean wind speed and potential temperature, and the intensity of the surface forcing, the vertical depth of the influence of surface heterogeneity varies (Mahrt, 2000). As shown in Fig.3, the spatial pattern of lower ABL potential temperature is consistent with the spatial pattern of surface radiation temperature (Fig. 1) and surface heat flux (Fig. 2). In addition, the potential temperature spatial pattern from the upper-level flight legs implies that the potential temperature pattern at 65 m AGL extends vertically to the ABL top (not shown).

The spatial distribution of ABL depth over the UWKA western track (Fig.4) is estimated from lidar aerosol backscatter data. On 19, 20, and 29 May, the ABL is deeper to the north and shallower to the south. This spatial pattern is altered on 25 May by the relatively elevated ABL depth around 36.60 N and local depression around 36.80 N latitude, consistent with the

observed patterns of surface temperature (Fig. 1) and surface kinematic heat flux (Fig. 2). On 7 June, rapid ABL growth across the entire track makes it difficult to find a consistent pattern in the ABL depth spatial distribution.

The horizontal distribution of water vapor mixing ratio at 65 m AGL and in the upper ABL both appear to be less consistent with the surface sensible heat and temperature patterns. This is consistent with the more transient structure in surface moisture fluxes. Spectral analyses show low-frequency structure in the water vapor fields that do not exist in the potential temperature fields.

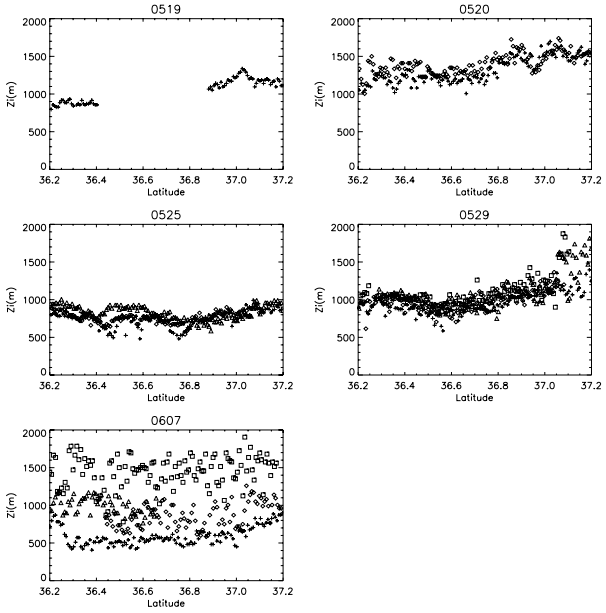

Fig. 4. Daytime ABL depths computed from aerosol backscatter measurements from the DLR water vapor differential absorption lidar on board the DLR Falcon.

4.3 Stationary Motions

The stationary spatial pattern of horizontal wind speed from the UWKA low-level flight legs is shown in Fig. 5. On 19, 20, and 29 May, when the spatial pattern of a warmer north and cooler south extended up to the ABL top, the horizontal wind magnitude decreases at 36.75 or 36.80 N. The wind direction is southerly or south-westerly. This deceleration of the horizontal wind is also apparent in the upper-level winds (not shown). The stationary distribution of wind direction exhibits a counterclockwise-turning at the northern end of the track. Furthermore, relatively large stationary upward vertical velocity is detected at the northern end of the track. The existence of a semi-permanent mesolow at the northern end of the flight track may cause this spatially persistent pattern.

Even though the mesolow is real, there can be other interpretations for the existence of this stationary motion. Stationary mesoscale circulations observed by LeMone et al. (2002) were mainly caused by terrain variability. On the UWKA western track, the maximum variation of surface elevation is 150 m. The lowest region at 36.80 N roughly corresponds to the convergence area on 19, 20, and 29 May with strong southerly (or west-southerly) background winds.

5. PRELIMINARY CONCLUSIONS AND PLANS

Persistent spatial patterns of potential temperature and sensible heat flux associated with heterogeneity in surface radiation temperature are observed. Since ABL depths exhibit a similar spatial pattern, this stationary variability of potential temperature likely extends through the depth of the ABL.

The interaction between land-surface heterogeneity and variable ABL structure cannot be correctly described without proper selection of the cutoff scale; that is, the minimum scale of surface heterogeneity that will alter the entire depth of the ABL. On 25 May, the day with lightest winds, this minimum length scale must be less than 25 km, as the heterogeneity both at surface and in ABL is poorly described using the 25 km segment averages. On windier days, 25 km segments averages describe the observed spatial patterns fairly well.

Moisture variability in the ABL seems to be less directly related to land-surface heterogeneity. Variance decomposition indicates the spatial patterns of surface moisture flux and water vapor mixing ratio at 65 m AGL are more transient than that of surface temperature, heat flux, and potential temperature.

This analysis also suggests the presence of stationary motions in the daytime ABL associated with surface heterogeneity on the UWKA western track. On 19, 20, and 29 May, a persistent stationary spatial pattern was apparent, with warm air to the north and cooler air to the south. The analyzed wind fields at 65 m AGL during these days imply the presence of convergence at the northern end of the UWKA western track. On 25 May when the region between 36.60 and 36.65 N is relatively warmer than on the other days and mean winds are very light, there is divergence on the northern part of the track.

Three-dimensional wind fields from the Doppler on Wheels (DOW) radars will be used to further analyze stationary spatial patterns in more detail than can be achieved with airborne in situ data. In addition the water vapor measurements from the DIAL (Differential Absorption Lidar) aboard the DLR Falcon will be used to further investigate the moisture structure in the ABL.

Acknowledgements

We thank Margaret A. LeMone for assistance with UWKA data analyses and for fruitful discussions. NCAR's Atmospheric Technology Division and UCAR's Joint Office for Science Support provided extensive support for IHOP. The DLR lidar group graciously provided backscatter data, and Ken Craig provided the ABL depth calculations based on these lidar data. This research is supported by a grant from the National Science Foundation's Atmospheric Sciences Division.

S. Kang was also supported by a Korean Government Fellowship

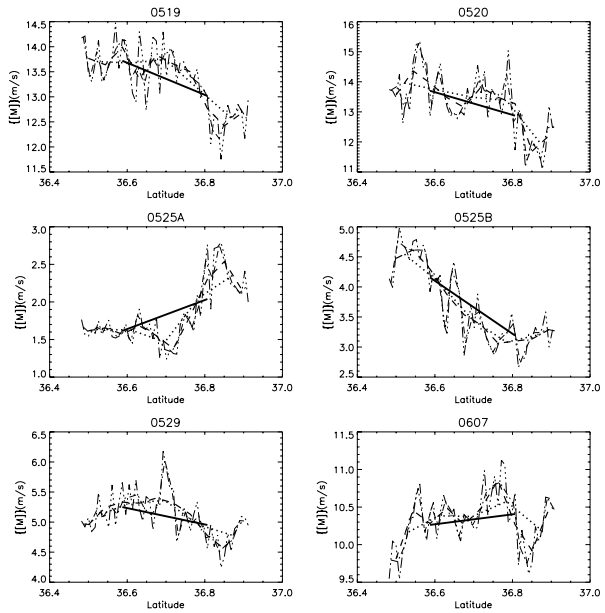

Fig. 5. Same as Fig.1, but for wind speed.

REFERENCES

Avissar, R., and Schmidt, T., 1998: An Evaluation of the Scale at which Ground-Surface Heat Flux Patchiness Affects the Convective Boundary Layer Using Large-Eddy Simulations. *J. Atmos. Sci.,* **55**, 2666-2689.

Davis, K. J., and Coauthors, 2000: An objective method for deriving atmospheric structure from airborne lidar observations. J. Atmos. Oceanic Technol., 17, 1455–1468.

Ehret, G., A. Fix, V. Weib, G. Poberaj, and T. Baumert, 1998: Diode-laser-seeded optical parametric oscillator for airborne water vapor DIAL application in the upper troposphere and lower stratosphere. Appl. Phys. B, 67, 427-431.

LeMone, M., and Coauthors, 2002 : CASE-97: Late-Morning Warming and Moistening of the Convective Boundary Layer over the Walnut River Watershed. *Bound.-Layer Meteor.*,**104**, 1-52

Mahrt, L, and Coauthors, 1994a: Observations of fluxes and inland breezes over a heterogeneous surface. *J. Atmos. Sci.,*51, 2484-2499.

Mahrt,L, J. I. Macpherson, and R. Desjardins, 1994b: Observations of fluxes over heterogeneous surfaces. Boundary.-Layer Meteor., 67, 345-367.

Mahrt, L., 2000: Surface heterogeneity and vertical structure of the boundary layer. *Bound.-Layer Meteor.*, 96, 33-62

Segal, M., and Arritt, R.W., 1992: Nonclassical Mesoscale Circulations Caused by Surface Sensible Heat-Flux Gradients. *Bull. Amer. Meteor. Soc.,* 73, 1593–1604.

Shen, S., and M. Y. Leclerc, 1995: How large must surface inhomogeneities be before they influence the convective boundary layer? A case study. Quart. J. Roy. Meteor. Soc., 121, 1209–1228.

Stull, R. B., 1988: *An Introduction to Boundary Layer Meteorology*. Kluwer Academic, 666 pp

Sun, J., and Coauthors, 1996: Scale Dependence of Air-Sea Fluxes over the Western Equatorial Pacific. *J. Atmos. Sci.,* 53, 2997-3012

Taylor, Christopher M., Saïd, Frédérique, Lebel, Thierry, 1997: Interactions between the Land Surface and Mesoscale Rainfall Variability during HAPEX-Sahel. *Mon. Wea. Rev.,* 125: 2211-2227

Weaver, P., and Avissar, R., 2001: Atmospheric Disturbances Caused by Human Modification of the Landscape. *Bull. Amer. Meteor. Soc.*,82: 269-282.

Weckwerth T. M., and Coauthors, 1996: Thermodynamic Variability within the Convective Boundary Layer Due to Horizontal Convective Rolls. *Mon. Wea. Rev*: 124, 769–784.

Weckwerth, T. M., and Coauthors, 2004: An Overview of the International H_2O Project (IHOP_2002) and Some Preliminary Highlights. *Bull. Amer. Meteor. Soc.,*85, 253-277